

Polarization Control for Slow and Fast Light in Fiber Optical, Raman-assisted, Parametric Amplification

M. Santagiustina, L. Schenato, C.G. Smeda

*Department of Information Engineering, University of Padova, via Gradenigo 6/B,
35131 Padova, Italy*

Abstract

Efficient slow and fast light fiber devices based on narrow band optical parametric amplification require a strict polarization control of the waves involved in the interaction. The use of high birefringence and spun fibers is studied theoretically, possible impairments evaluated, and design parameters determined.

Key words:

PACS: 42.81.Gs Birefringence, polarization, 42.65.Yj Optical parametric oscillators and amplifiers, 42.81.Wg Other fiber-optical devices

1. Introduction

It has been demonstrated that narrowband optical parametric amplification (NBOPA) is a superb technique for inducing slow and fast light (SFL) in optical fibers [1]. Large group delay tuning, over selectable, wide frequency bands, makes this technique a very promising candidate for many envisaged applications. Record tunable SFL delays of communication digital data signals were achieved in dispersion shifted fibers (DSF) [1]. In particular, experimental demonstrations were performed for 10 Gbit/s and theoretical predictions for 40 Gbit/s digital signals have been given [2, 3].

Theoretical studies resulted into a good understanding of the NBOPA, SFL process and its intrinsic limitations [1, 4] under the key assumption of an ideal homogeneous, isotropic fiber. However, real fibers are not likely to be homogeneous nor isotropic, and NBOPA gain and delay are affected by the longitudinal variations of the fiber linear propagation parameters such

as the zero dispersion wavelength (ZDW) fluctuations [5] and the random birefringence [6].

Fluctuations of the ZDW cause gain broadening and thus a decrease in the achieved delay. The main contribution to ZDW shifts comes from changes in the fiber core effective area occurring during the drawing process [7, 8], so ZDW shift is not time varying. Eventually, the ZDW shift can be measured [5, 7] and the gain broadening can be highly mitigated by selecting uniform samples, and by increasing the pump power.

The polarization sensitivity of optical parametric interactions is a much more intriguing issue [9, 10]: the parametric gain coefficient is maximum when the pump and the signal have the same state of polarization (SOP), while it vanishes for orthogonal SOPs. So, maintaining a strict control of the pump and signal relative SOPs along the fiber is a critical issue for attaining reliable SFL devices based on NBOPA.

The most widespread fibers (i.e. telecommunication ones) are not isotropic, though their birefringence is very low (here, they will be referred to as low birefringence - LoBi - fibers). The residual birefringence stems from the manufacturing imperfections (e.g. small asymmetries of the fiber core circular section) and from the fiber operating conditions (e.g. stresses, bending, twisting and temperature changes) due to environmental conditions; all these factors eventually break the polarization degeneracy of the fundamental mode, and the fiber becomes birefringent. The residual, stochastic, low birefringence causes a random phenomenology known as polarization mode dispersion (PMD) [11, 12]. The parametric interaction is very sensitive to PMD, that modifies the pump, signal and idler SOPs in a random fashion along the fiber [13]. Detailed analyses of the effects of PMD on NBOPA gain and SFL delay can be found in refs. [14, 15, 16]. The effect is very pronounced and harmful because: a) it increases with the signal-pump frequency detuning, which is very large for NBOPA [17]; b) differently from ZDW fluctuations, which are deterministic, PMD is a random, time varying phenomenon [11, 12].

In this contribution, two special fiber types that can be used to control the polarization of waves interacting in a NBOPA, SFL device will be theoretically and numerically studied. The paper aims at presenting fundamental design information for improving the NBOPA, SFL fiber devices beyond the present state of the art. High birefringence (HiBi) fibers, in which the SOP is maintained [18], are an obvious choice to mimic the isotropic ideal case, but not the only one. Significant reductions of random polarization effects in

Raman [19], Brillouin [20] and parametric [21, 22] amplifiers, have been recently predicted when unidirectionally spun (US) fibers are considered. Here, the weight of possible negative effects in HiBi fibers and the positive effects of unidirectional spinning for on NBOPA-SFL are quantified.

The paper is organized as follows. In section 2 the equations describing the NBOPA with polarized fields, in different fiber types, are introduced. The main features of propagation in LoBi, HiBi and US fibers will be also recalled in this section. In section 3 the performance in LoBi fibers will be assessed. The study of NBOPA, SFL in HiBi and US fibers will be carried out in sections 4 and 5, respectively. Finally, conclusions will be drawn in section 6.

2. Propagation model

The aim of this section is to provide a unified model to describe the NBOPA propagation for different fiber types, e.g. LoBi, HiBi and US. Moreover, the main features of the propagation of optical signals in such fiber types will be also reviewed.

Let us define $|A_p(z)\rangle$, $|A_s(z, t)\rangle$, $|A_i(z, t)\rangle$, the Jones vectors of the pump, signal and idler waves respectively. For detailed definitions of the ket $|\rangle$ symbol and the bracket operators $|\rangle\langle|$, $\langle|$, one can refer to [12].

In the undepleted pump approximation, neglecting the nonlinear effects of the signal and idler on the pump and by considering a continuous wave pump, the equations governing the nonlinear interaction of the slowly varying envelopes for the pump, signal and idler read [14, 15, 16, 23, 24]:

$$\begin{aligned} \frac{d|A_p\rangle}{dz} &= [\mathcal{L}_p + \mathcal{S}_p(|A_p\rangle)] |A_p\rangle, \\ \frac{\partial|A_s\rangle}{\partial z} &= [\mathcal{L}_s + \mathcal{X}_s(|A_p\rangle) + \mathcal{R}_s(|A_p\rangle)] |A_s\rangle + \mathcal{F}_s(|A_p\rangle) |A_i^*\rangle \\ \frac{\partial|A_i\rangle}{\partial z} &= [\mathcal{L}_i + \mathcal{X}_i(|A_p\rangle) + \mathcal{R}_i(|A_p\rangle)] |A_i\rangle + \mathcal{F}_i(|A_p\rangle) |A_s^*\rangle. \end{aligned} \quad (1)$$

The operators $\mathcal{L}_{p,s,i}$ account for the linear propagation properties, while \mathcal{S}_p , $\mathcal{X}_{s,i}$, $\mathcal{R}_{s,i}$, $\mathcal{F}_{s,i}$ are operators that depend on the pump wave $|A_p\rangle$, and take into account the nonlinear effects that are relevant for each wave, i.e. self-phase modulation, cross-phase modulation, Raman scattering and four-wave mixing. The linear operators are described in this section, as the different

fiber type (LoBi, HiBi, US) properties are dictated by these operators. Non-linear operators present very complicated structures, that are described in the Appendix 8, for the sake of completeness.

The linear operators are defined as:

$$\mathcal{L}_h = -\alpha_h + j\beta_h - \beta_{1h} \frac{\partial}{\partial t} - j \frac{1}{2} \bar{\beta}(\omega_h) \cdot \bar{\sigma} + \frac{1}{2} \bar{\delta}_h \cdot \bar{\sigma} \frac{\partial}{\partial t}, \quad h = p, s, i. \quad (2)$$

In eqs. 2, $\alpha_{p,s,i}$ are the loss coefficients, $\beta_{p,s,i} = \beta(\omega_{p,s,i})$ the mean wavenumbers at the optical angular frequencies of the pump, signal and idler $\omega_{p,s,i} = 2\pi c_0/\lambda_{p,s,i}$ satisfying $2\omega_p = \omega_s + \omega_i$. The nonlinear phase matching condition to be satisfied is: $2\beta_p - \beta_s - \beta_i = \Delta\beta = \beta_{2p}(\omega_s - \omega_p)^2 + \beta_{4p}(\omega_s - \omega_p)^4/12 = -2\gamma P_0$, where β_{np} is the n -th derivative of $\beta(\omega)$ with respect to the angular frequency, calculated at ω_p [25], and $P_0 = \langle A_p(0)|A_p(0) \rangle$ is the input pump power. The parameters used in the following simulations are: ZDW, $\lambda_0 = 1.5423 \mu\text{m}$; $\lambda_p = 1.53 \mu\text{m}$; $\beta_{2p} \simeq \beta_{30}(\omega_p - \omega_0)$; $\beta_{30} = 1.14 \cdot 10^{-40} \text{ s}^3/\text{m}$; $\beta_{4p} = -5 \cdot 10^{-55} \text{ s}^4/\text{m}$; $P_0 = 1 \div 5 \text{ W}$. Then, the NBOPA phase matched wavelengths are: $\lambda_s \simeq 1.3927 \mu\text{m}$, $\lambda_i \simeq 1.7096 \mu\text{m}$.

If the reference frame (z, t) used in eqs. 1 is travelling at the signal group velocity $v_g(\omega_s)$, one also gets $\beta_{1h} = 0$, for the signal ($h = s$) and $\beta_{1h} = 1/v_g(\omega_s) - 1/v_g(\omega_i)$ for the idler ($h = i$).

The effects of fiber birefringence are accounted for by the last two terms of the operator (2). In the first term the Stokes vector $\bar{\beta}(z, \omega)$ is the local birefringence vector that describes the birefringence at each point within the fiber; $\bar{\sigma}$ is the vector of the Pauli spin matrices [12]. In the second term: $\bar{\delta}_h = \partial\bar{\beta}/\partial\omega$ calculated at ω_h [23].

Results for an ideal, isotropic fiber, can be obtained by setting $\bar{\beta} = 0 \forall z, \forall \omega$. In real fibers, the properties of the birefringence vector, which change from one type to the other, are very important. For this reason, they need to be specified in detail.

For LoBi (unspun) fibers $\bar{\beta}(z, \omega) = \bar{\beta}_{un}(z, \omega) = [\beta_1, \beta_2, 0]$ is a random vector. Its evolution along z can be obtained by means of the so-called random modulus model (RMM) [26], i.e. its components are generated by the following Langevin equations:

$$\frac{d\beta_i}{dz} = -\rho\beta_i + \nu\eta_i, \quad i = 1, 2 \quad (3)$$

where β_i ($i = 1, 2$) are Gaussian stochastic variables of zero mean and variance $\nu_\beta^2 = \nu^2/(2\rho)$ and $\eta_i(z)$ for $i = 1, 2$ are independent, Gaussian white

noises of zero mean and unitary variance. Note that $\beta_3(z) \equiv 0$ is set in the numerical solutions, as is commonly assumed [26] and experimentally verified in most cases [27]. This condition means that the fiber does not exhibit any circular birefringence.

In the RMM, PMD is actually described by two length scales: the beat length $L_B = 2\pi/(\sqrt{2}\nu_\beta)$, and the birefringence correlation length $L_F = 1/\rho$. The former depends on the frequency ($L_B(\omega) = \omega_0 L_B(\omega_0)/\omega$) and describes the length scale of polarization changes, while the latter is frequency independent ($L_F = 9$ m in our simulations), and accounts for the length scale of birefringence changes. Both lengths contribute to determine the PMD coefficient [26], hereinafter defined as $D = \sqrt{\langle \Delta\tau^2 \rangle / L}$, where $\langle \Delta\tau^2 \rangle$ is the fiber mean square differential group delay (DGD), and L is the fiber length. The DGD is defined as the time delay between pulses, at the same carrier frequency, launched along the two principal states of polarization (PSPs) [28] in LoBi fibers, and along the birefringence axes in HiBi fibers. The PSPs are defined as those input SOPs whose corresponding output SOPs are frequency independent at first order [28]. The typical coefficient D , in LoBi fibers, ranges from 10^{-2} ps/ $\sqrt{\text{km}}$, for low PMD fibers, to more than 10^{-1} ps/ $\sqrt{\text{km}}$ for high PMD ones.

The second type of fibers, HiBi, are for example realized by inducing internal stresses (PANDA fibers) or by making an asymmetric core (elliptical core fibers). In both cases the large intrinsic guide birefringence, voluntarily introduced during the manufacturing process, dominates over random effects. Then, in HiBi fibers the linear birefringence vector $\bar{\beta}$ has a predominant, deterministic, linear contribution $\bar{\beta}_{HiBi}$ whose modulus is related to the DGD $\Delta\tau$ by $|\bar{\beta}_{HiBi}| = c_0 \Delta\tau / (\lambda L)$. Input SOPs parallel to birefringence axes ($\pm \hat{\beta}_{HiBi} = \pm \bar{\beta}_{HiBi} / |\bar{\beta}_{HiBi}|$) are polarization eigenstates, and so they travel unchanged through the entire fiber length. For this reason HiBi fibers are also referred to as polarization maintaining (PM) ones. Though the deterministic birefringence is overwhelming, random mode coupling along the fiber still exists. Furthermore, input misalignment may also result in a nonvanishing cross-polarized orthogonal SOP. The tolerance of the SFL technique with respect to SOP misalignment has been investigated and will be discussed in the following. Moreover, for a more realistic simulation of the unwanted effects, a random component, described again by the RMM, has been added to the deterministic part of the birefringence $\bar{\beta} = \bar{\beta}_{HiBi} + \bar{\beta}_{ran}$ [11]. The value of D has been chosen to yield the typical polarization cross-talk ratio (PXR)

[29] of commercial HiBi fiber, always better than 20 dB. As for the effects of input misalignments, the delay was calculated numerically exploring all possible linear input SOPs.

Finally, US fibers have been considered; fiber spinning is a manufacturing process routinely performed while drawing fibers from LoBi preforms. In particular, periodic spinning functions, in which the fiber is turned alternatively clockwise and counterclockwise, are often applied to reduce external stresses and fiber PMD [30]. Unidirectional spinning, besides reducing the DGD, has been predicted to enhance the SOP alignment of optical signals at different frequencies, in particular in nonlinear fiber amplifiers [19, 20, 21, 22]. The birefringence vector of a spun fiber can be obtained from that of the unspun case through the transformation $\bar{\beta}(z, \omega) = R_3[2\phi(z)]\bar{\beta}_{un}(z, \omega)$ where R_3 is a Mueller matrix representing a rotation around the third axis in the Stokes space (\hat{u}_3). For an US fiber the angle of rotation is given by the constant spin function $\phi(z) = 2\pi z/p$, where p is called the spin pitch. It has been shown [31] that when $p^2 \ll L_B^2$, the polarization properties of the US fiber can be effectively described by a simplified model (SM). In the SM, the fiber can be represented by an equivalent birefringence vector, with a random linear and a deterministic circular component:

$$\bar{\beta}_{eq}(z) = (\sqrt{2\mu}\xi_1(z), \sqrt{2\mu}\xi_2(z), -\chi)^T, \quad (4)$$

where $\xi_i(z)$ are statistically independent Gaussian white noises and the moduli of the linear and circular components are given by:

$$\mu = \frac{2L_F(\pi p)^2}{L_B^2[p^2 + (4\pi L_F)^2]}, \quad \chi = \frac{4\pi L_F\mu}{p}. \quad (5)$$

The results of the SM are recalled here because in section 5 they will contribute to explain the mitigation of polarization effects .

For LoBi and US fibers, several hundreds statistical realizations of the stochastic processes, and subsequent integrations of eqs. 1, have been realized to calculate the mean gain and time delay.

To conclude this section, let us remark that when propagation in birefringent media is considered, the group velocity cannot be uniquely defined, as observed by Haus [32]. Exceptions are represented by the special cases in which the input SOPs coincide with the PSPs, in LoBi fibers, or birefringence axes, in HiBi fibers. In those two cases, a different value is found for the group velocity for each PSP or axis. In all other conditions, the standard

formula $\Delta T_g = d(\beta z)/d\omega = z/v_g(\omega)$ for the group delay loses its physical significance. Hence, in the numerical integrations, the group delay ΔT_g has been evaluated as the first moment of the pulse as a function of time [15, 33] (the input pulse was Gaussian, 70 ps FWHM)

$$\Delta T_g(z) = \frac{\int t \langle A_s(z, t) | A_s(z, t) \rangle dt}{\int \langle A_s(z, t) | A_s(z, t) \rangle dt} \quad (6)$$

In particular, the difference between the arrival time when the SFL pump is on and when it is off, ($\Delta T = \Delta T_g^{on} - \Delta T_g^{off}$), is calculated according to this definition.

3. Low birefringence fibers

Let us first briefly review the effects of PMD on SFL propagation in NBOPA [14, 15, 16]. For LoBi fibers the loss of alignment between signal and pump SOPs causes a reduction of the mean gain, which in turn translates into a delay reduction. For small PMD coefficients the mean delay $\langle \Delta T \rangle$ can be calculated with the ideal isotropic case formula [4, 16], where the gain is replaced by the mean gain, i.e.:

$$\begin{aligned} \langle \Delta T \rangle = & L\sqrt{6k_2} \sqrt{\frac{1}{L_D}} \sqrt{1 + \frac{2}{3} \frac{L_D}{\langle L_{NL} \rangle}} \sqrt{1 + \sqrt{1 + \frac{2}{3} \frac{L_D}{\langle L_{NL} \rangle}}} \times \\ & \times \left[1 - \frac{\langle L_{NL} \rangle}{L} \tanh \left(\frac{L}{\langle L_{NL} \rangle} \right) \right] \end{aligned} \quad (7)$$

where $L_D = -\beta_{4p}/\beta_{2p}^2$ and the mean nonlinear length $\langle L_{NL} \rangle$ is related to the mean gain $\langle G \rangle$ by:

$$\frac{L}{\langle L_{NL} \rangle} = \cosh^{-1} \left(\sqrt{\langle G \rangle} \right). \quad (8)$$

For larger random birefringence, strong pulse distortion sets in, and the delay decreases faster than the gain. Though mean quantities follow the ideal relation, random birefringence causes a large uncertainty in the actual delay. This fact can be easily grasped from fig. 1, where the NBOPA gain versus delay, for many realization of an unspun fiber, for a PMD coefficient $D = 0.05$ ps/ $\sqrt{\text{km}}$, is shown and compared with the case (squares) for $D = 0$ (ideal

isotropic fiber). In the real case, PMD shifts the phase-matching condition [14, 16], and therefore the gain is reduced, while eq. 7 is still valid. As we said, the delay standard deviation, represented by vertical red bars, is very large; around 20 – 30 ps i.e. almost 50 percent of the mean achieved delay. Finally, pulses are affected by a severe distortion. The large fluctuations of the delay are probably the most detrimental impairment introduced by PMD. So, regardless of LoBi fibers being the most commonly used ones, using them for making stable NBOPA based SFL devices is highly hampered.

4. High birefringence fibers

For SFL in HiBi fibers, the key parameter is power splitting among polarizations. In the ideal case, since birefringence axes are eigenpolarizations, no cross-polarization coupling occurs if signal and pump are co-polarized, and aligned along $\pm\hat{\beta}_{HiBi}$ at the fiber input. Under real conditions, however, some coupling always exists because of input misalignment, either of the signal or of the pump, with respect to the birefringence axes, and/or because of small imperfections in the fiber. Therefore, the robustness of the SFL scheme against input misalignments has been tested. The main results are summarized in fig. 2.

The delay was first calculated as a function of the polarization misalignment between the (linear) signal SOP and the fast fiber axis ($+\hat{\beta}_{HiBi}$), along which the pump is supposed to be launched (empty circles). As we see, the delay is essentially unaffected for almost all signal SOP misalignments; it decreases significantly only when the signal is launched almost orthogonally. The explanation of the small change in delay is that a large polarization dependent gain is generated in this case [15]; therefore, the signal polarization is attracted, by a nonlinear polarization pulling effect similar to that described for Brillouin and Raman amplification [34, 35]), towards the direction yielding maximum gain. In practice, the portion of the signal pulse polarized along the minimum gain direction (slow axis) is weakly amplified, so that the pulse center of mass actually coincides with that of the powerful pulse component on the fast axis. When the pump and signal SOPs are orthogonal (i.e., 90 degrees misalignment) there is no gain, and consequently no SFL effect. Hence, the delay tends to coincide with that due to linear birefringence. This has been verified by propagating the signal pulse without the pump (solid line); as the misalignment between the signal and the fast axis increases, more signal power is launched on the slow axis, and delayed

because of the different group velocities. A mirror-like behavior is observed if we launch the pump on the slow axis (squares in fig. 2). In this case the delay is the sum of the SFL induced delay and that due to the change in the signal propagation axis.

The effects of the pump input SOP misalignment are shown in fig. 2 (empty diamonds). As more pump power is launched on the slow axis, orthogonally to the signal, the gain, and consequently the delay, decrease; both tend to zero when the misalignment tends to 90 degrees. Remarkably, there are certain input pump SOP's for which the delay becomes negative. This stems from the fact that the input signal wavelength is left constant, at the phase matching condition obtained when the pump is launched on the fast axis. But as the effective pump power decreases because of the misalignment, the phase matching condition shifts, and consequently the signal spectrum is now in a frequency band where the delay is negative. This explanation has been verified by calculating the delay with the ideal exact formula (i.e. eq. 9 of [16]); the results are presented in fig. 2 by the dashed curve.

We may conclude that the delay reduction due to signal and pump input misalignment with respect to fiber axis is negligible, if the angle is less than 10 degrees, an easy condition to satisfy in practice.

Finally, we considered the random coupling, bearing in mind that this is a very small effect in good-quality HiBi fibers. Typically the PXR, i.e. the ratio between power on orthogonal axes at the output of 100m of fiber, is better than 20 dB. To evaluate these effects of the residual random coupling on the SFL delay, a stochastic component, obtained through RMM, was added to the deterministic linear birefringence vector, so that the total vector becomes: $\bar{\beta} = \bar{\beta}_{HiBi} + \bar{\beta}_{ran}$. The value of D was chosen such that the probability of getting realizations with a PXR in excess of 20 dB was very low. The results of a set of statistical realizations of this random process show that the maximum spread in the time delay is less than 1 percent of the mean value, very close to the ideal value. We conclude that the effect of the residual random coupling on SFL delay is negligible in HiBi fibers.

5. Unidirectionally spun fibers

Last, the case of US is considered. Fig. 3 shows a statistical set of realizations of a fiber with the same value of D as in fig. 1, but spun with a pitch $p = 2$ m. We see that the delay standard deviation is greatly reduced, and gets down to 5 ps. An impressive reduction of the standard deviation is

obtained by further decreasing the pitch, as shown in fig. 4, where $p = 0.5$ m. Note that there is no longer a significant difference with respect to the case of an ideally isotropic fiber.

This remarkable result can be explained by the fact that in US fibers, as the spin pitch decreases, the equivalent deterministic circular birefringence and the random linear birefringence decrease. This is shown in fig. 5, where the strengths of the random linear and deterministic circular components of the equivalent vector are calculated from eqs. 5. It is then clear that US fibers behave similarly to ideal isotropic fibers, when the spin pitch is short enough. The final outcome is that the pump and signal SOPs remain almost parallel, for all possible SOPs launched at the fiber input.

The enhanced parallelism is illustrated also by figs. 6 and 7, where the mean value of $\cos(\theta_{p,s})$ ($\theta_{p,s}$ being the angle between the signal and pump SOPs in Stokes space, at the fiber output) is shown for the two cases (unspun and US), as a function of detuning from the signal carrier frequency. Note that the alignment increases as the spin pitch decreases; moreover, it increases with pump power. The latter effect is, once again, an indication of the nonlinear polarization pulling effect that we mentioned in the previous section [34, 35].

6. Conclusions

The problem of how to control the SOP of the signal and pump, for slow and fast light in narrow-band, Raman-assisted, optical parametric amplification, has been studied theoretically and numerically. It was shown that standard, unspun telecommunication fibers can exhibit delay fluctuations, caused by polarization mode dispersion, that are too large in order to yield reliable slow and fast light effects for practical applications.

To mimic an ideal isotropic fiber, two options have been explored: high birefringence fibers, and unidirectionally spun fibers.

For HiBi polarization maintaining fibers, the typical achievable polarization crosstalk ratio is sufficiently good to guarantee that an isotropic-fiber like delay is obtained. The effects of practical signal input misalignments are also under control, thanks to the nonlinear polarization pulling effect, which attracts the signal SOP towards the direction yielding maximum gain. Furthermore, small input pump misalignments, to be expected in practice, are not affecting the delay to a significant level.

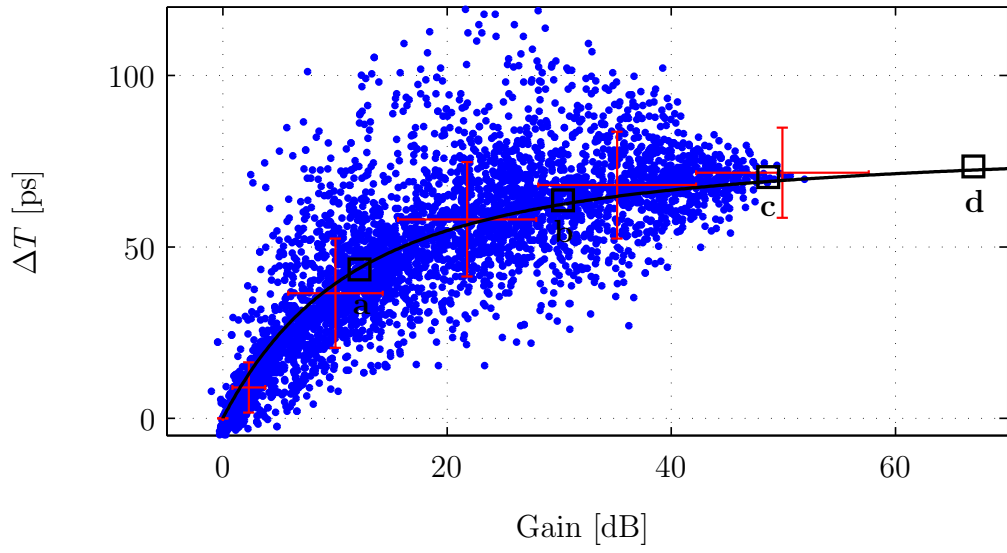


Figure 1: Delay vs. gain from the numerical solutions of eqs. 1 ($L=1\text{km}$) for P_0 : a) 1 W; b) 2 W; c) 3 W; d) 4 W. Squares, isotropic fiber ($D = 0$); dots, LoBi fiber ($D = 0.05$ ps/ $\sqrt{\text{km}}$); solid line, eq. 7. Bars define the gain and delay standard deviation; their crossing point is the mean value.

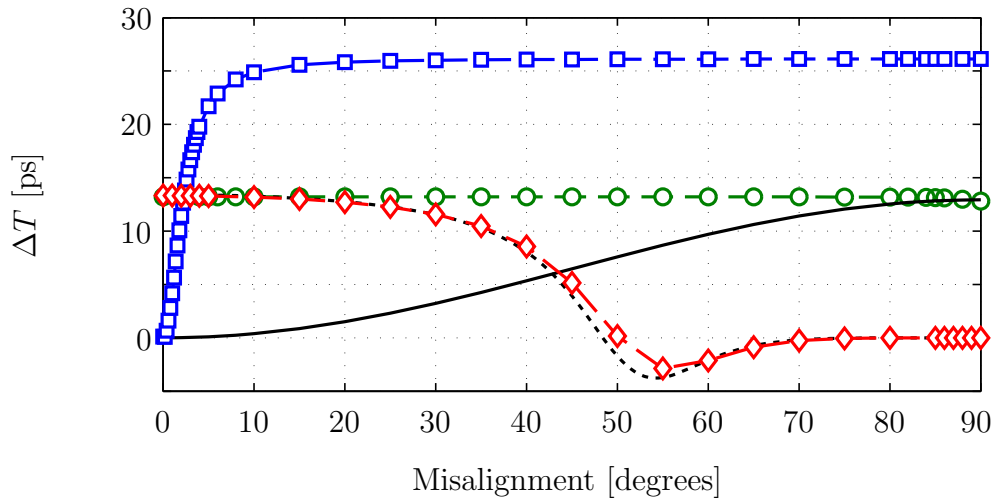


Figure 2: Delay vs. input misalignment. Signal - fast axis misalignment: Solid curve, no pump; Circles, pump aligned with the fast axis; Squares, pump aligned with the slow axis. Pump - fast axis misalignment: Diamonds, signal aligned with the fast axis; Dashed curve, analytical result.

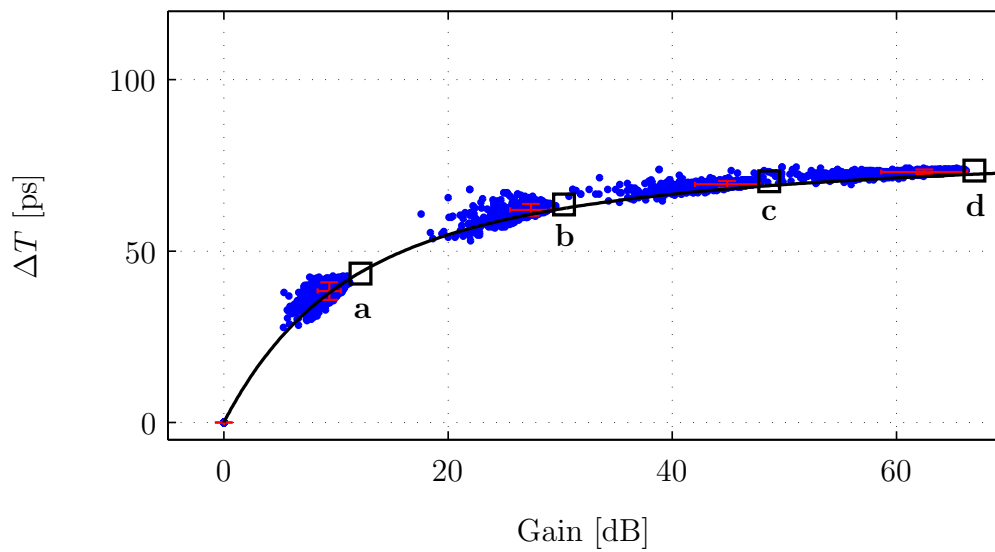


Figure 3: Same as fig. 1, but for a US fiber, $p = 2 m$.

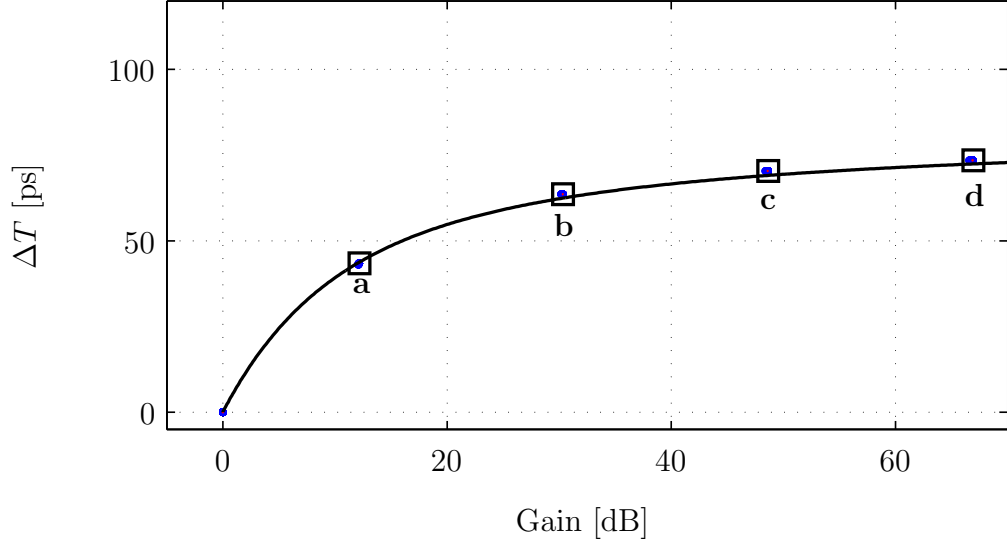


Figure 4: Same as fig. 1, but for a US fiber, $p = 0.5$ m.

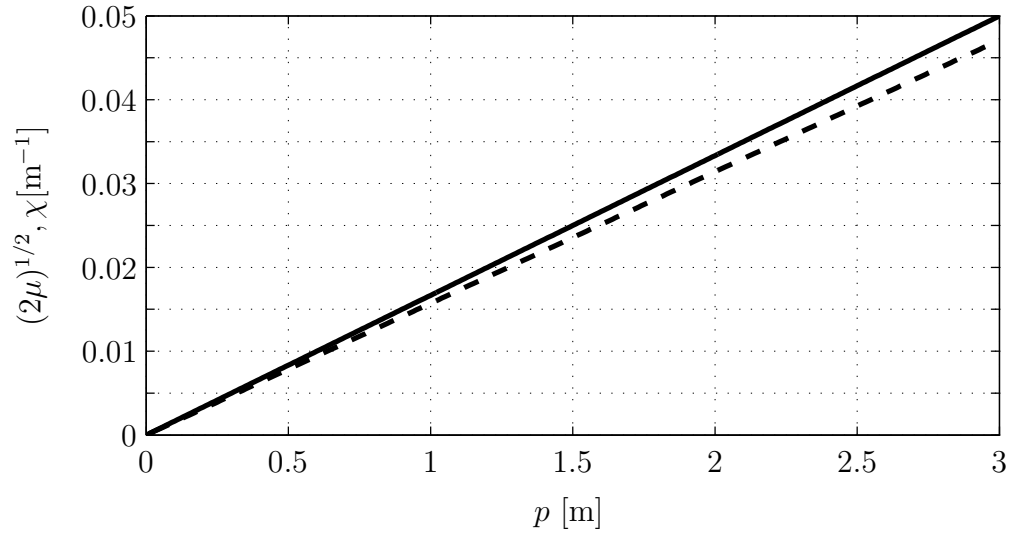


Figure 5: Strength of the SM equivalent birefringence vector components, $\sqrt{2\mu}$ (linear, dashed line) and χ (circular, solid line), as functions of the spin pitch p , as from eqs. 5 ($L_B = 10$ m, $L_F = 9$ m).

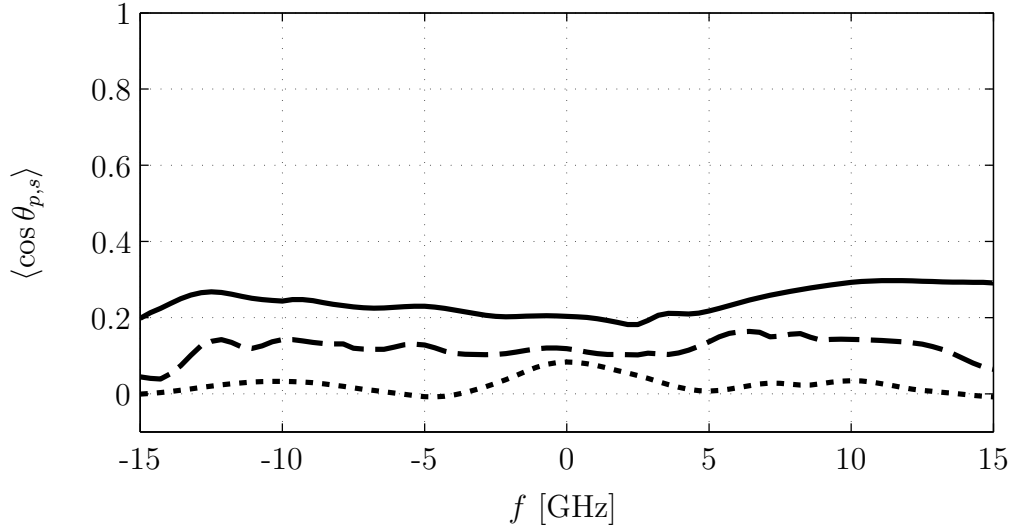


Figure 6: Alignment factor $\cos(\theta_{p,s})$ between the output signal and pump SOPs in Stokes space, as a function of the frequency detuning from signal carrier frequency for a LoBi fiber; dotted, dashed and solid curves are for $P_0 = 1, 3, 5$ W respectively.

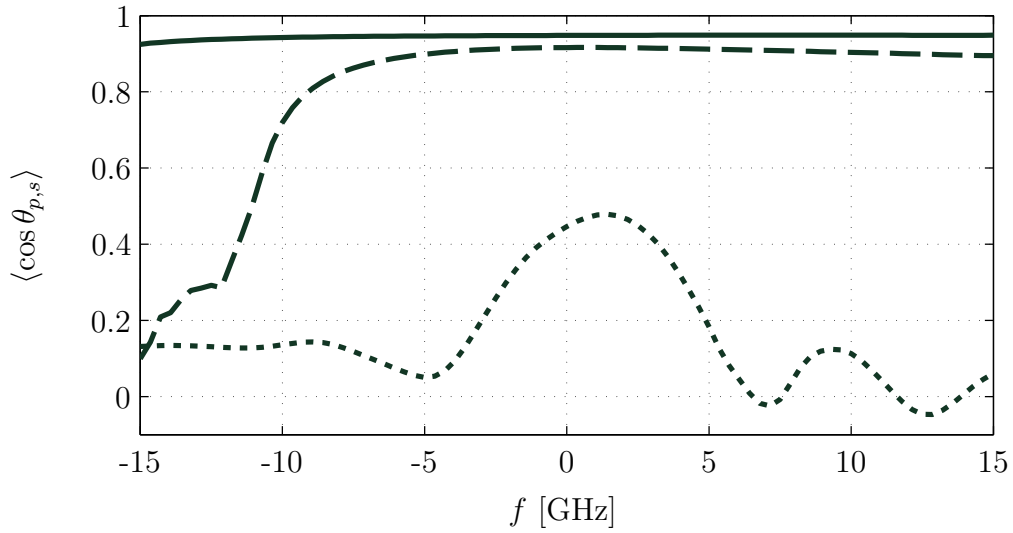


Figure 7: Same as fig. 6, but for a US fiber, $p = 2$ m.

Finally, unidirectionally spun fibers were considered. For fast spinning (0.5 m), they have been shown to behave essentially like ideal isotropic fibers. In fact, compared to unspun fibers, the polarization mean alignment is highly enhanced along the entire length of the fiber. An additional advantage of spun fibers is that they maintain aligned *any* state of polarization, so the only care they require is to align signal and pump at the fiber input along the same direction.

From a practical viewpoint, high birefringence commercial fibers are readily available, though customization might be necessary for tailoring the dispersion properties to match the typical wavelengths of pump sources. As for unidirectionally spun fibers, spin pitches down to a few mm are feasible with present technologies. Therefore, such fibers could indeed be the most suitable tools for implementing reliable, wideband, slow and fast light devices.

7. Acknowledgments

The research leading to these results has received funding from the European Community's Seventh Framework Programme (FP7/2007-2011). under grant agreement n 219299 "GOSPEL". Part of this work was done within the agreement between the University of Padova and ISCOM, Rome, Italy. Part was supported by the Italian Ministry of Foreign Affairs (Direzione Generale per la Promozione e la Cooperazione Culturale).

8. Appendix

The nonlinear operators of eqs. 1 are defined accordingly to the following expressions:

$$\begin{aligned} \mathcal{S}_p &= j \frac{\gamma_p^{NR}}{3} [2\langle A_p | A_p \rangle \mathbf{I} + |A_p^* \rangle \langle A_p^*|] + \\ &+ j [(\chi_{p,1212}^R(0) + \chi_{p,1122}^R(0)) \langle A_p | A_p \rangle \mathbf{I} + \chi_{p,1221}^R(0) |A_p^* \rangle \langle A_p^*|] \end{aligned} \quad (9)$$

$$\mathcal{X}_{s,i} = 2j \frac{\gamma_{s,i}^{NR}}{3} [\langle A_p | A_p \rangle \mathbf{I} + |A_p \rangle \langle A_p| + |A_p^* \rangle \langle A_p^*|] \quad (10)$$

$$\begin{aligned} \mathcal{F}_{s,i} &= j \frac{\hat{\gamma}_{s,i}^{NR}}{3} [\langle A_p^* | A_p \rangle \mathbf{I} + 2|A_p \rangle \langle A_p^*|] + \\ &+ j [(\hat{\chi}_{s,i,1122}^R(\Omega) + \hat{\chi}_{s,i,1221}^R(\Omega) - \hat{\chi}_{s,i,1212}^R(\Omega)) \langle A_p^* | A_p \rangle \mathbf{I} + \\ &+ (2\hat{\chi}_{s,i,1212}^R(\Omega) + \hat{\chi}_{s,i,1122}^R(\Omega) + \hat{\chi}_{s,i,1221}^R(\Omega) \\ &- \hat{\chi}_{s,i,1122}^R(0) - \hat{\chi}_{s,i,1221}^R(0)) |A_p \rangle \langle A_p^*|] \end{aligned} \quad (11)$$

$$\begin{aligned} \mathcal{R}_{s,i} &= j [2\chi_{s,i,1122}^R(\Omega) \langle A_p | A_p \rangle \mathbf{I} + 2\chi_{s,i,1212}^R(\Omega) |A_p \rangle \langle A_p| + \\ &+ 2\chi_{s,i,1221}^R(\Omega) |A_p^* \rangle \langle A_p^*|] \end{aligned} \quad (12)$$

where

$$\gamma_p^{NR} = \frac{2\pi\omega_p^2}{c^2\beta_p A_p} \chi_{1122}^{NR}, \quad (13)$$

$$\gamma_{s,i}^{NR} = \frac{2\pi\omega_{s,i}^2}{c^2\beta_{s,i} A_{s1,i1}} \chi_{1122}^{NR}, \quad (14)$$

$$\hat{\gamma}_{s,i}^{NR} = \frac{2\pi\omega_{s,i}^2}{c^2\beta_{s,i} A_{s2,i2}} \chi_{1122}^{NR}, \quad (15)$$

with

$$\chi_{1111}^{NR} = 3\chi_{1212}^{NR} = 3\chi_{1122}^{NR} = 3\chi_{1221}^{NR}, \quad (16)$$

and

$$\chi_{p,klmn}^R(\Omega) = \frac{2\pi\omega_p^2}{c^2\beta_p A_p} \chi_{klmn}^R(\Omega), \quad (17)$$

$$\chi_{s,i,klmn}^R(\Omega) = \frac{2\pi\omega_{s,i}^2}{c^2\beta_{s,i} A_{s1,i1}} \chi_{klmn}^R(\Omega), \quad (18)$$

$$\hat{\chi}_{s,i,klmn}^R(\Omega) = \frac{2\pi\omega_{s,i}^2}{c^2\beta_{s,i} A_{s2,i2}} \chi_{klmn}^R(\Omega), \quad (19)$$

with

$$\chi_{1111}^R(\Omega) = \chi_{1212}^R(\Omega) + \chi_{1122}^R(\Omega) + \chi_{1221}^R(\Omega). \quad (20)$$

and

$$\Omega = \omega_p - \omega_i = \omega_s - \omega_p. \quad (21)$$

The expression of the nonresonant components of the nonlinearity coefficient χ_{klmn}^{NR} and of the resonant components of the nonlinear Raman susceptibility $\chi_{klmn}^R(\Omega)$ can be found in [24]. The effective areas A_p and $A_{s1,i1}$, $A_{s2,i2}$ read

$$A_p = \frac{\langle f_p^2 \rangle^2}{\langle f_p^4 \rangle}, \quad (22)$$

$$A_{s1,i1} = \frac{\langle f_p^2 \rangle \langle f_{s,i}^2 \rangle}{\langle f_p^2 f_{s,i}^2 \rangle}, \quad (23)$$

$$A_{s2,i2} = \frac{\langle f_p^2 \rangle \sqrt{\langle f_s^2 \rangle} \sqrt{\langle f_i^2 \rangle}}{\langle f_p^2 f_s f_i \rangle}, \quad (24)$$

where here angle brackets stand for integrals over the trasversal modal profiles $f_j = f_j(x, y)$ ($j = p, s, i$). In the numerical simulation of this paper it has been assumed $A_p = A_{s1,i1} = A_{s2,i2}$.

References

- [1] D. Dahan, G. Eisenstein, "Tunable all optical delay via slow and fast light propagation in Raman assisted fiber optical parametric amplifier: a route to all optical buffering", *Opt. Expr.* 16, 6234-6249 (2005).
- [2] E. Shumakher, R. Blit, A. Willinger, D. Dahan, G. Eisenstein, "Large tunable delay with low distortion of 10Gbit/s data in slow light system based on narrow band fiber parametric amplification", *Opt. Expr.* 14, 8540-8545 (2006)
- [3] E. Shumakher, R. Blit, A. Willinger, D. Dahan, G. Eisenstein, "Large Delay and Low Distortion of a 40 Gbit/s Signal Propagating in a Slow Light System Based on Parametric Amplification in Optical Fibers", *ECOC 2006*, We4.3.4 (2006)

- [4] M. Santagiustina, L. Schenato, C. G. Someda, “Fundamental limit of the achievable time delay in Slow-Light NB-OPA”, *IEEE-LEOS Winter Topicals Conference 2008*, TuB1.5 (2008).
- [5] E. Shumakher, A. Willinger, G. Eisenstein, “High Resolution Extraction of Fiber Propagation Parameters for Accurate Modeling of Slow Light Systems Based on Narrow Band Optical Parametric Amplification”, *OFC 2007*, OTuC2 (2007)
- [6] M. Santagiustina, C. G. Someda, L. Schenato, L. Palmieri, A. Galtarossa, E. Bettini, “Optical Parametric Amplification for Slow Light in Random Birefringence Fibers”, *IEEE Photonics in Switching 2007*, TuB1.2 (2007).
- [7] M. Eiselt, R.M. Jopson, R.H. Stolen, “Nondestructive position-resolved measurement of the zero-dispersion wavelength in an optical fiber”, *J. Light. Tech.* 15, 135-143 (1997).
- [8] M. Karlsson, “Four-wave mixing in fibers with randomly birefringent zero-dispersion wavelength”, *JOSA B* 9, 2269-2275 (1998).
- [9] M.E. Marhic, K.K.Y. Wong, L.G. Kazovsky, “Fiber optical parametric amplifiers with linearly or circularly polarized waves”, *JOSA B* 20, 2425-2433 (2003).
- [10] Q. Lin, G.P. Agrawal, “Vector theory of four-wave mixing: polarization effects in fiber-optic parametric amplifiers”, *JOSA B* 21, 1261-1224 (2004).
- [11] G.J. Foschini, C.D. Poole, “Statistical theory of polarization mode dispersion in single mode fibers”, *J. Light. Tech.* 9, 1439 (1991).
- [12] J. P. Gordon, H. Kogelnik, “PMD fundamentals: Polarization mode dispersion in optical fibers”, *Proc. Natl. Acad. Sci.* 97, 4541 (2000).
- [13] Q. Lin, G.P. Agrawal, “Effects of polarization-mode dispersion on fiber-based parametric amplification and wavelength conversion”, *Opt. Lett* 29, 1114-1116 (2004).
- [14] A. Willinger, E. Shumakher, G. Eisenstein, “On the role of polarization and Raman assisted phase matching in narrow band fiber parametric amplifiers”, *J. Light. Tech.* 26, 2260-2268 (2008).

- [15] G. Eisenstein, E. Shumakher, A. Willinger, “Slow and fast light propagation in narrow band Raman-assisted fiber parametric amplifiers”, in *Slow Light: Science and Applications*, J. B. Khurgin and R.S. Tucker, Eds., CRC Press, 2008, 149-172.
- [16] L. Schenato, M. Santagiustina, C.G. Someda, “Fundamental and random birefringence limitations to delay in slow light fiber parametric amplification”, *J. Light. Tech.* 26, 3721-3726 (2008).
- [17] L. Schenato, M. Santagiustina, C. G. Someda, “Narrow Band Optical Parametric Amplification for Slow Light in Randomly Birefringent Fibers”, *OFC 2008*, JThA3 (2008).
- [18] H.G. Park, J.D. Park, S.S. Lee, “Pump-intensity-dependent frequency shift in Stokes and anti-Stokes spectra generated by stimulated four-photon mixing in birefringent fiber”, *Appl. Opt.* 26, 2974-2978 (1987).
- [19] E. Bettini, A. Galtarossa, L. Palmieri, M. Santagiustina, L. Schenato, L. Ursini, “Polarized Backward Raman Amplification in Unidirectionally Spun Fibers”, *IEEE Phot. Tech. Lett.* 20, 27-29 (2008).
- [20] A. Galtarossa, L. Palmieri, M. Santagiustina, L. Schenato, L. Ursini, “Polarized Brillouin amplification in randomly birefringent and unidirectionally spun fibers”, *IEEE Phot. Tech. Lett.* 20, 1420-1422 (2008).
- [21] H. Ferraro, A. Galtarossa, L. Palmieri, M. Santagiustina, L. Schenato, “Unidirectionally Spun Fibers for Efficient Narrow-Band Parametric Amplification”, *OFC 2009*, JWA14 (2009).
- [22] M. Santagiustina, L. Schenato, “Parametric Amplification in Randomly Birefringent and Spun Fibers”, *IEEE Phot. Tech. Lett.*, submitted (2009).
- [23] Q. Lin, G.P. Agrawal, “Effects of polarization-mode dispersion on cross-phase modulation in dispersion-managed wavelength-division-multiplexed systems”, *J. Light. Tech.* 22, 977-987 (2004).
- [24] S. Trillo, S. Wabnitz, “Parametric and Raman amplification in birefringent fibers”, *JOSA B* 9, 1061 (1992).

- [25] M.E. Marhic, N. Kagi, T.K. Chiang, L.G. Kazovsky, “Broadband fiber-optical parametric amplifiers”, *Opt. Lett.* 21, 573-575 (1996).
- [26] P.K.A. Wai, C.R. Menyuk, “Polarization mode dispersion, decorrelation and diffusion in optical fibers with randomly varying birefringence”, *J. Light. Tech.* 14, 148-157 (1996).
- [27] A. Galtarossa, L. Palmieri, M. Schiano, T. Tambosso, “Measurement of birefringence correlation length in long single-mode fibers”, *Opt. Lett.* 26, 962-964 (2001).
- [28] C.D. Poole, R.E. Wagner, “Phenomenological approach to polarisation dispersion in long single-mode fibres”, *Electr. Lett.* 22, 1029-1030 (1986).
- [29] J. Noda, K. Okamoto, Y. Sasaki, K. Okamoto, “Polarization-maintaining fibers and their applications”, *J. Lightwave Technol.* 4, 1071-1089 (1986).
- [30] A.J. Barlow, J.J. Ramskov-Hansen, D.N. Payne, “Birefringence and polarization mode-dispersion in spun single-mode fibers”, *Appl. Opt.*, vol. 20, 2962-2968, 1981.
- [31] L. Palmieri, “Polarization properties of spun single-mode fibers”, *J. Lightwave Technol.* 24, 4075-4088 (2006).
- [32] H. Haus, “Group velocity, energy, and polarization mode dispersion”, *JOSA B* 16, 1863-1867 (1999).
- [33] R.L. Smith, “The velocities of light”, *Am. J. Phys.* 38, 978-984 (1970).
- [34] A. Zadok, E. Zilka, A. Eyal, L. Thevenaz, M. Tur, “Vector analysis of stimulated Brillouin scattering amplification in standard single-mode fibers”, *Opt. Exp.* 16, 21692-21707 (2008).
- [35] M. Martinelli, M. Cirigliano, M. Ferrario, L. Marazzi, P. Martelli, “Evidence of Raman induced polarization pulling”, *Opt. Exp.* 17, 947-955 (2009).